The Pennsylvania State University

The Graduate School

STUDY OF LASER-INDUCED GRAPHENE SILVER NANOWIRE TRIBOELECTRIC NANOGENERATORS

A Thesis in

Engineering Science and Mechanics

by

Daniel J. Erdely

Submitted in Partial Fulfillment
of the Requirements
for the Degree of

Master of Science

May 2022

The thesis of Daniel J. Erdely was reviewed and approved by the following:

Huanyu Cheng
Assistant Professor of Engineering Science and Mechanics
Thesis Advisor

David Snyder
Assistant Professor, IGDP Material Science and Engineering

Melik Demirel
Lloyd and Dorothy Foehr Huck Chair in Biomimetic Materials
Director, Center for Research on Advanced Fiber Technologies

Albert Segall
Professor and Graduate Programs Officer
Program Head

ABSTRACT

The on-body wearable sensor field is a rapidly growing area of research that has much promise. One of the biggest problems to solve for their effectiveness is how they are powered. So far, the traditional methods of taking the device off the body and charging them with a cable have been used, which means data is lost while the device needs to charge. In the past, an effect known as triboelectrification has been used to provide continuous power by converting mechanical energy into electrical energy. These devices have been limited to traditional fabrication methods like electrospinning[1] and single-layer graphene growth[2] or limited electrode area to achieve flexibility.[3] Here, three separate laser-induced graphene (LIG) and polydimethylsiloxane (PDMS) triboelectric nanogenerators (TENGs) were developed and tested to find an improved energy harvesting method. The first was constructed with simply LIG and PDMS. The second was built the same as the first but with silver nanowires (AgNWs) to aid electron transfer. Lastly, the third TENG was fabricated with AgNWs and crumpled LIG to increase the surface area of the surfaces in contact. The smooth LIG TENG had an output of 280nA but degraded quickly due to the LIG adhering to the PDMS. The smooth LIG/AgNW had the best output of 333nA due to the improved conductivity that the AgNWs provided. Finally, the crumpled LIG/AgNW TENG had the lowest output of 75nA because the size of the crumpled structure was too large, actually decreasing the contact surface area and thus output. While these results are lower than reported literature values for similar LIG TENGs, it proves that a crumpled LIG TENG can be created and provide a foundation for crumpled LIG TENGs in the future.

TABLE OF CONTENTS

LIST OF FIGURES

LIST OF TABLES

Acknowledgments

This thesis would not have been possible without the incredible support of the following people. The determination of everyone involved is what kept progress moving forward in the second year of a global pandemic.

Dr. Huanyu Cheng for allowing me to do this master's thesis and offering me support and guidance.

Dr. Naveen Tiwari who has been my primary source of help throughout this process and has always been available to discuss any problems I had.

Dr. Yuyan Gao helped me get this research off the ground initially and provided insight into using the linear stage.

Abu Musa Abdullah for helping me set up the rectifier circuit and work on the oscilloscope.

Jackson Nicastro for assisting in Matlab plotting, data processing, and coding.

My family and friends for being a constant source of motivation and support throughout the entire thesis process.

Chapter 1

Introduction

1.1 Motivation and Scope

As humanity becomes more health-conscious every passing year, wearable devices such as the Apple Watch or Fitbit become more mainstream. Creating better health monitoring devices and powering them becomes more critical. Besides the sensing capabilities of the devices, they lack reliable ways for the devices to be powered continuously so that they never have to be taken off the body for recharging. One way to do this is through an energy harvesting method that is reliable, efficient, and durable that can provide sufficient and continuous power to these devices. TENG is a device that allows for energy harvesting from the mechanical energy of everyday activities such as walking or even typing on the computer. A TENG device needs to be easily fabricated, comfortable to wear, and easily conform to the body without degrading performance. Because of that, no reliable TENG has been fabricated using crumpled LIG as the basis of a TENG that allows for reliable energy harvesting. Fabricating a flexible and stretchable crumpled device made from LIG has not been done yet because LIG is very brittle compared to chemical vapor deposition graphene.

This research lays out a first attempt to fabricate a crumpled LIG TENG with AgNWs. Three different devices are created based on three different structures to show the difference in performance between the devices and a path forward for improvement.

1.2 Impact

The impact of this research reaches into many different domains, and its impact can be far-reaching. First, the most significant impact of the TENG will be on the energy industry and how any electrical device is charged. Generating electricity by simply contacting or sliding two materials together will allow people to keep their electronic devices charged for longer. Additionally, this constant power source will allow for continuous health monitoring devices. These can be glucose monitors used for people with diabetes or any other wearable health monitoring devices such as EMG or ECG. These devices would revolutionize human health care by providing continuous monitoring of a person's health that can be used to predict and prevent disease and illness.

Furthermore, since people are using their movement for a source of electricity, it will make them less reliable on the power grid, thus saving them money and causing the power companies to lose money and eventually making them obsolete. Ethically, these devices need to be biocompatible if used on humans, and the necessary safety trials must be completed with the relevant organizations. Safety needs to be the top priority when doing any research in the lab.

Chapter 2

Literature Review

2.1 Laser-Induced Graphene

Since the creation of LIG in 2014 by lasing a polymer sheet with a CO_2 laser, the space of LIG has grown drastically, and the technology has applications in numerous wearable device sectors from micro supercapacitor arrays, triboelectric nanogenerators, and even sweat sensors.[4][5][6][7] These devices are possible due to this method being easily scalable, rapidly repeatable, able to generate unique shapes and create a highly porous and conducting graphene structure. This process occurs by photothermally converting the sp^3 carbon atoms into sp^2 carbon atoms. The creation of LIG is a photothermal process due to the longer wavelength of 10.6μm and the longer pulse duration. The longer pulse duration is the opposite of a photochemical process when polymers are laser ablated. The highly concentrated energy of the laser on the polymer causes local temperatures of over 2,500°C because of the increase in lattice vibrations. This highly concentrated energy can also be observed through fluorescence from the polymer at every pulse of the laser. The carbon-oxygen single and double bonds and the nitrogen-carbon bonds can be broken at high temperatures. Once the bonds are broken, the oxygen and nitrogen atoms recombine as gases and are vented away from the surface. Once the oxygen and nitrogen atoms are vented away, the only remaining atoms are over 90% carbon if the laser power is below 4.2W. Otherwise, oxidation becomes an increasingly important factor in improving the conductivity of the LIG. Furthermore,

through RAMAN spectra and TEM imaging, a good ratio of D/G intensity peaks shows strong carbonization of the polyamide (PI) film. The hexagonal structure of the LIG is observed in TEM images while also showing the randomness of hexagonal graphene structures.[8]

LIG cannot be produced on just any polymer but depends on the type of monomer or polymer present in the chain and how the chain was formed. Aromatic and imide compounds must be present in a step-growth polymer such as PI or poly(ether imide) in order for LIG to be created. Aromatic compounds must be present because the aromatic cyclic compounds reform to create the LIG. The formation of LIG is not restricted to solely polymers, however. LIG can be created on wood in inert gas conditions and on other organic materials such as potato skins or even bread due to the high lignin content present in those materials.

The highly porous structure and conducting nature of LIG allow it to be used in various ways. The highly porous structure allows different nanoparticles to be embedded in the crevices of the graphene that then give the LIG enhanced material properties. With the addition of Ag nanoparticles in the LIG, the sheet resistance is significantly reduced, allowing it to be used in a rectenna device. While LIG is not stretchable when attached to the PI sheet, it can be easily transferred to a stretchable polymer such as PDMS to allow it to be used in stretchable electronic devices and as a basis for electrodes for strain sensors.[9][10]

2.1.1 Crumpled Laser-Induced Graphene

Since LIG can be easily transferred to an elastomeric substrate, it can use different strategies to form structures usually reserved for thin films. One of these structures is forming a crumpled pattern of the LIG through two different methods. The first is a common strategy that relies on prestraining an elastomeric substrate such as PDMS and then transferring the LIG to the prestrained substrate. Then the strain is released, and the LIG buckles locally on the PDMS. The buckling of the LIG allows for what usually is brittle LIG to be stretchable without a loss in resistance.[7] In order to achieve this structure without any breaks in the crumpled LIG, high laser power is needed of 45W. The high laser power produces poorly formed LIG, evidenced by the high sheet resistance of 200Ω/sq, where LIG is typically ~25 Ω/sq.[9]

The other method for creating a crumpled LIG morphology is printing the LIG on an already crumpled film. A crumpled film of polyether ether ketone was 3D printed to achieve consistent spacing between the crumples. Then the laser was rastered over the film at a consistent height even though the film was not planar. The advantage of this technique is that a low sheet resistance is attainable, which is characteristic of LIG printed on a planar surface. The two major drawbacks of this technique are that since the height of the laser is not varied based on the morphology of the crumples, the quality of LIG is different from the peaks to the valleys. Also, since the LIG was not formed using a pre-strain strategy, the buckled structure forms cracks in the valleys when the LIG is stretched. These cracks form with stretching as small as 10%, which limits the robustness of the structures.[11]

2.2 Buckled Structures

The idea of buckled structures to increase surface area for thin films and increase stretchability in the semiconductor industry has been around for over 15 years. It relies on the simple idea of adhering a film to a strained substrate and then releasing the strain, causing local buckling of the film on the substrate. Models have been developed to predict the amplitude and wavelength of the buckling structure. The first models predict the amplitude and wavelength for small prestrain, so the equations are independent of the prestrain ε_{pre}. The equation for the wavelength can be seen below in Equation (1). The variables are defined as the following: h is the thickness of the thin film, $\bar{E}_f$ is the plane-strain modulus of the thin film, $\bar{E}_s$ is the plane-strain modulus of the substrate. According to Equation (2), the plane strain modulus is defined where E is the elastic modulus and v is the Poisson ratio.[12]

$$\lambda_o = 2\pi h \left(\frac{\bar{E}_f}{3\bar{E}_s} \right)^{1/3} \quad (1)$$

$$\bar{E} = E/(1 - v^2) \quad (2)$$

The amplitude is similarly defined as the wavelength using approximations for small deformations in the thin film in Equation (3). In this case ε_{pre} is the strain applied to the substrate before the thin film adheres to it. ε_c in Equation (3) is defined according to Equation (4). It is the minimal strain that needs to be applied to the substrate to cause the thin film to buckle when the strain is released.[12]

$$A_o = h \sqrt{\frac{\varepsilon_{pre}}{\varepsilon_c} - 1} \quad (3)$$

$$\varepsilon_c = \frac{1}{4}\left(\frac{3\bar{E}_s}{\bar{E}_f}\right)^{2/3} \quad (4)$$

Since Equation (1) and Equation (3) are independent of the amount of pre-strain applied to the substrate, they give very different results compared to experiments. Once the pre-strain percent of the substrate goes past 10%, these equations are no longer helpful and overestimate the wavelength and amplitude of the buckles. Therefore, more inclusive equations were developed to account for the substrate's pre-strain and the unevenness of the geometry of the film-substrate interface. These equations also still see the buckling as purely sinusoidal, just like Equation (1) and Equation (3). They use the existing amplitude and wavelength defined in Equation (1) and Equation (3). The updated equation for the wavelength is seen below in Equation (5). ξ is defined in Equation (6) and depends purely on the pre-strain of the substrate. This equation was used to predict the buckling of a Si thin film on PDMS, and it agreed with the experimentation without manipulating the data.[12]

$$\lambda = \frac{\lambda_o}{(1+\varepsilon_{pre})(1+\xi)^{1/3}} \quad (5)$$

$$\xi = \frac{5\varepsilon_{pre}(1+\varepsilon_{pre})}{32} \quad (6)$$

Similarly, as the wavelength, the updated amplitude is defined below in Equation (7). This Equation agrees equally as well with the data gathered from experimentation as Equation (5).[12]

$$A = \frac{A_o}{\sqrt{1+\varepsilon_{pre}}(1+\xi)^{1/3}} \quad (7)$$

The equations above have been modified and applied to predict more complex buckling structures such as biaxially strained substrates that form herringbone shapes.[13][14] Also, controlled delamination of certain areas of the thin film is possible to create structures known as nanoribbons.[15] Both of these more advanced strategies allow increased flexibility for different electronic applications. These buckled structures are also used to create optical gratings that can be modified to change the optical transmittance of transparent substrates.[16]

The strategy of creating buckled structures is not restricted solely to the semiconductor industry. It has also been applied to more novel materials such as graphene[17][2][5] or Ag nanoparticles embedded in PDMS.[3] The increased surface area that is possible with the buckling increased the output of graphene-based TENGs due to an increase in charge transfer between the electrodes. Furthermore, crumpled graphene was used to create a strain sensor using solely crumpled graphene.[5]

2.3 Triboelectric Nanogenerators

The phenomena of contact electrification and static electricity have been known for centuries. Contact electrification or triboelectrification, in particular, occurs when two different materials exchange charges. While contact electrification has been known for centuries and triboelectrification for decades, the fundamental physics driving the transfer of charges between two materials is not fully understood. This is because these charge transfers happen on the atomic scale, and characterization techniques do not exist yet that are capable of accurately characterizing the processes taking place on that scale. The

three prevailing hypotheses behind the charge transfer mechanism involve electrons, ions in the form of protons and hydroxide ions, and the transferring of the material. The electron transfer model was widely accepted at first because it was based on the transferring of charges between two semiconductors or a semiconductor and a metal. This model of work functions and energy band diagrams was applied to insulator-insulator charge transfer in TENGs. However, since the bandgap of insulators is much higher than semiconductors and metals, the charges would have to overcome a very large thermal energy kT. The high thermal energy would make the transfer of charges between insulators very unlikely, even though experimentally, they are better triboelectric materials than metals and semiconductors. There have been attempts to resolve this problem, using theories such as an interfacial layer and measuring the triboelectric process between polymers using atomic force microscopy. On the other hand, the ion transfer model hypothesizes that mobile ions could be responsible for triboelectrification. This model depends on the presence of H^+ and OH^- ions absorbed into the surface of ionic and nonionic polymers. H^+ and OH^- ions redistribute themselves when two nonionic polymers are contacted using the nature of the "water-bridge" model. This model has been partly validated because of the positive correlation of ions in the polymer and the charge measured on the polymer.[18] This model has also been slightly disproven when TENGs were tested in zero-humidity environments, and electrical output was still observed but was reduced.[19] Finally, direct observation of charged nanoscale particles being transferred between two materials has been observed. This model could help explain the charging between two identical materials where the electron and ion transfer models do not hold up because the charges would be homogenous throughout. However,

the mechanism behind charge transfer in triboelectric materials is still unresolved. Combining the three models presented above could work in unison to make the triboelectric effect happen.[18]

The extent to which the materials build up these surface charges during contact depends heavily on the materials chosen and their polarity. Because of this, triboelectric series have been created to help researchers determine which materials build up the most surface charge when contacted together.[20] While these series are comprehensive, the list of available triboelectric materials is short, so the surfaces of these existing materials are being altered by halogens and amines to tailor the triboelectric properties of a single material.[21] Metal-organic frameworks are also being used to lower the degree to which metal-ion coupling occurs, which can significantly improve the output of TENGs.[22]

The fundamental physics of the triboelectric process has been studied extensively through theoretical models[23] by looking at environmental factors such as humidity and pressure on the performance of TENGs.[24] The theoretical models determined an equation for the optimal load resistance depending on the materials chosen for the TENG. More recently, the density of states was studied as another determining factor of triboelectric charge generation. The group created a density of states model based on different polymers to picture triboelectric charge generation better. Their work discovered that while polyethylene terephthalate (PET) is more negative on the triboelectric series, the charge generated per unit area is lower than Kapton, which is less triboelectrically negative. They determined this was due to the high density of states present in Kapton compared to PET.[25]

One standard way the voltage output of TENGs is measured is by connecting the two electrodes of a TENG to an oscilloscope, with one of those leads being connected to the ground. While this usually gives a good picture of the voltage output of the TENG, grounding one electrode could lead to a loss in the measured open-circuit voltage of the TENG since that voltage is going straight to the ground and not being measured. A group looked at a method to measure the voltage of a TENG without grounding one electrode to get the proper open-circuit voltage of TENGs. They accomplished this by connecting two voltmeters back-to-back in series and got a twofold voltage output for the non-grounded method compared to the grounded.[26]

With all of this background, it was not until 2012, however, that the first triboelectric nanogenerator was created.[27] It was a flexible design that relied on rubbing two rough surfaces together to produce opposite charges and thus produce a current. There have been many ways the triboelectric effect is produced from that point on. The triboelectric effect is produced using one or two electrodes by sliding materials through friction, sliding without contact, and solely contacting two materials together.[18] These different modes have been incorporated into many areas and combined with other energy harvesting techniques such as piezoelectricity.[28], [29] There are trapezoidal-shaped TENGs with a cantilever design that are designed to work at higher frequencies such as 15Hz in applications where those range of frequencies are already being produced.[30] This frequency response has been studied to determine the optimal frequency to maximize output in a TENG.[31]

The application of TENGs is also wide-reaching and broad. A group made unique conducting yarns to incorporate a TENG into a textile with nylon.[32] It showed very

high repeatability and durability, surviving over 40 wash cycles. TENGs have been incorporated into the world of renewable energy harvesting as well. Another group created a tower TENG that resembles a buoy to harvest the energy of waves in the ocean. It contains polytetrafluoroethylene (PTFE) balls that roll around on the inside of the tower generating electricity.[33] Other methods, such as using a thin film fluorinated ethylene propylene sheet in contact with water, have also been demonstrated to harvest energy from waves.[34] Besides energy harvesting from waves, TENGs are used to produce electroluminescence by sliding a PDMS surface doped with ZnS: Cu over PTFE to drive electroluminescence.[35] They are being incorporated into monitoring different aspects of sports such as heart rate or even swimming strokes by attaching a TENG to the elbow of a swimmer.[36] More recently, TENGs have started to use graphene[37] and even LIG[37] to create double-sided smart bracelets to power devices[39], as well as being the power source for LIG-based biosensing platforms.[3]

Chapter 3

Smooth LIG Based Triboelectric Nanogenerator

3.1 Fabrication of Smooth LIG based TENG

The first step of fabricating this device was to create the LIG. The LIG was created using a 30W Universal Laser System VLS 2.30 CO_2 laser. Initially, a piece of 180µm polyimide (PI) tape was cut to an adequate size to fit the 2cm x 2cm electrode and was stuck to a glass slide or flat piece of metal. The process parameters of the laser were determined from trial and error to obtain the best transfer process of the LIG onto the 3M VHB tape. Those parameters were 19% for the laser power, 11% for the laser speed, and 1000 PPI. The thickness of this LIG was 43µm, as can be seen in Figure **3-1** below. The raster pattern of the laser can be seen in Figure **3-1** below as well.

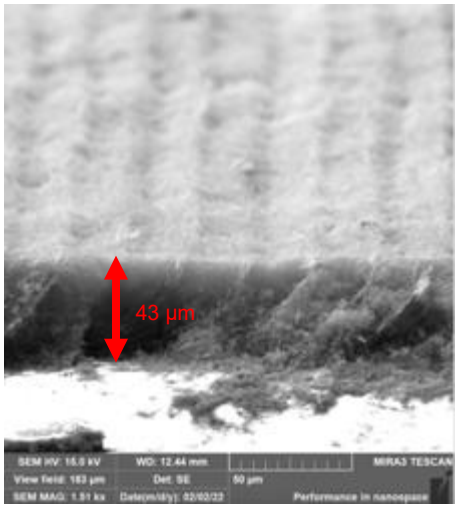

Figure **3-1**: Thickness of as printed LIG on PI film.

A top-down view of the LIG was also captured using a Keyence optical microscope with ring lighting at different magnifications. In Figure **3-2a,** a wide-angle image was taken showing an overall view of the structure, and in Figure **3-2b,** a more magnified image at 100x was captured to clearly show the laser's pattern. Once the LIG was fabricated in Figure **3-3a**, it was transferred to a piece of 4910 3M VHB tape Figure **3-3b**. The transfer process was done by cutting a big enough piece of VHB tape and then placing it on top of the LIG. Next, a clamp was used to apply pressure between the VHB and LIG for a few minutes. The clamp was then removed, and starting from one corner; the VHB was peeled off in one quick motion with the LIG firmly bound to the surface Figure **3-3c**. After this transfer, the sheet resistance across this newly fabricated electrode was tested to ensure the LIG had appropriately transferred with no gaps. The sheet resistance was measured using the transfer line method (TLM). These were done using a Keithley 4200 and probe station with a -5V to 5V sweep to measure the resistance. Six different lengths were fabricated for these measurements. The sheet resistance measurements depending on the raster pattern before and after transferring can be seen below in Table **3-1**. The long raster sheet resistance was 10.7Ω before transferring and 18.8Ω after transferring to the 3M VHB tape.

On the other hand, the short raster direction had a higher sheet resistance of 17.1 Ω before transferring and then 28.2 Ω after transferring to the 3M VHB tape. The long raster measurement refers to the laser rastering lengthwise, and the short raster refers to the laser rastering widthwise. The complete data from these measurements can be seen in Figure **A-1,** Figure **A-2,** Figure **A-3,** Figure **A-4.** The two different rastering directions

were done to study the difference in resistance between the two directions to understand how the charges would flow across the electrode.

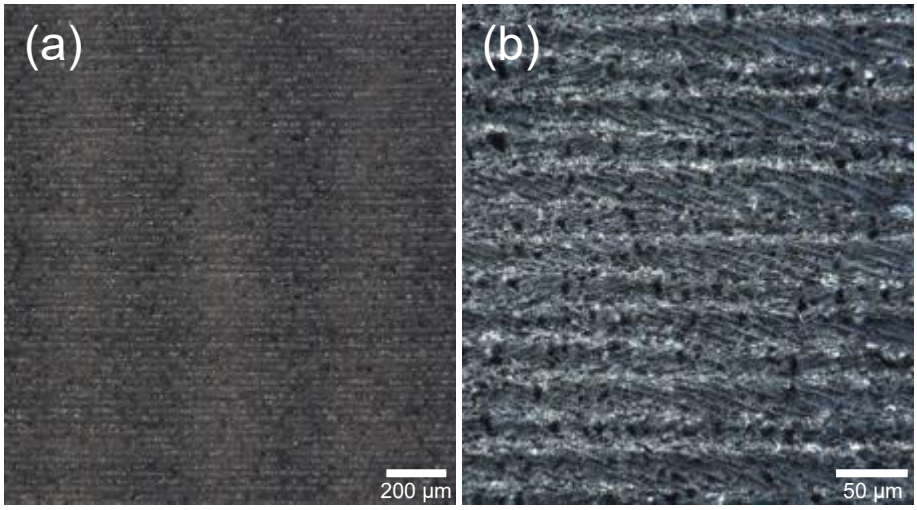

Figure **3-2**: (a) Optical image of LIG printed on PI film at 20x. (b) Optical image of LIG printed on PI film at 100x.

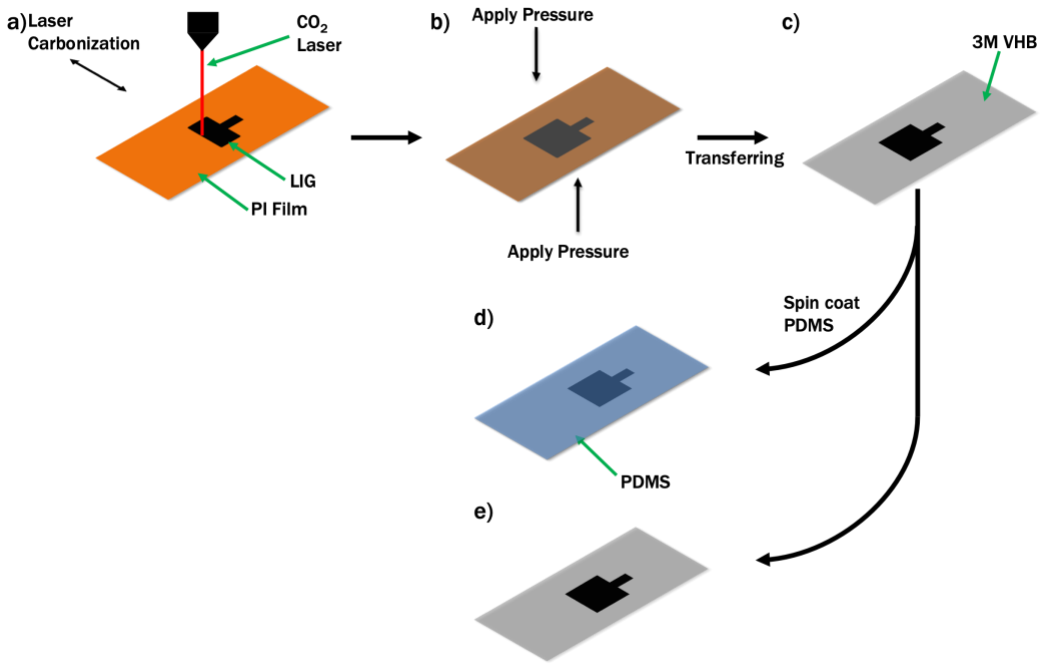

Figure **3-3**: Fabrication process of the smooth LIG TENG

Table **3-1**: Resistance of LIG electrodes on 3m VHB tape from various spots on the electrode.

Long Raster (Ω)	Short Raster (Ω)	Long Raster Transferred (Ω)	Short Raster Transferred (Ω)
10.7	**17.1**	**18.8**	**30.0**

SEM images of the transferred LIG were captured to further study this slight increase in resistance. The images in Figure **3-4a** and Figure **3-4b** were captured using an SEM and show microscopic cracks in the LIG on the order of 25-50μm spaced every 200μm across the surface. Also, small cracks can be seen in between the larger cracks in Figure **3-4a**. Furthermore, the porosity of the LIG is maintained even after transferring, which is evidenced by Figure **3-4b** and Figure **A-5.** The thickness of the LIG after transferring also increased to ~75μm Figure **A-6**. The reason for this will be discussed further in the discussion section.

Next, each electrode of the two electrode TENG was created. The first step was to make a stable contact to ensure accurate output readings with minimal loss. A simple Ag paste and copper foil contact were fabricated on the LIG electrode's top section. The contacts were made by first mixing a small portion of the two-part Ag paste and applying it to the protruding part of the electrode. Next, a small strip of copper foil was pressed onto the Ag paste. The paste was then let to dry at room temperature overnight to ensure complete drying of the paste. The resistance was then checked to ensure a good contact was created.

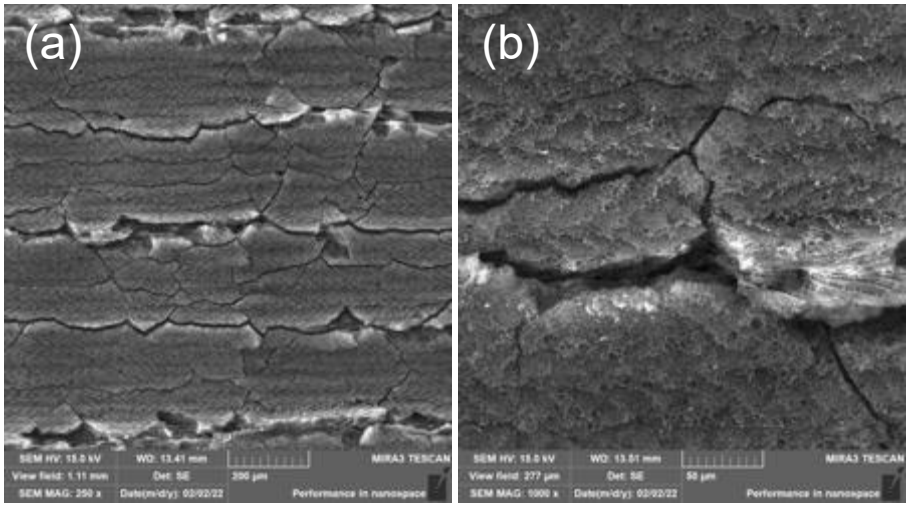

Figure **3-4**: (a) Structure of transferred LIG on unstrained VHB tape 250x. (b) Structure of transferred LIG on unstrained VHB tape 1000x.

Next, the two electrodes were fabricated. One of the electrodes required no further fabrication Figure **3-3d**. It was attached to a flat piece of polymethyl methacrylate (PMMA) to give it a rigid back and ensure contact between the two electrodes. The other was spin-coated with a thin layer of a two-part PDMS called Ecoflex 30 Figure **3-3e**. The PDMS covered the entire electrode and had a uniform thickness of ~80μm, as seen in Figure **3-5**. The two fully fabricated electrodes are seen in Figure **3-6a** and Figure **3-6b**.

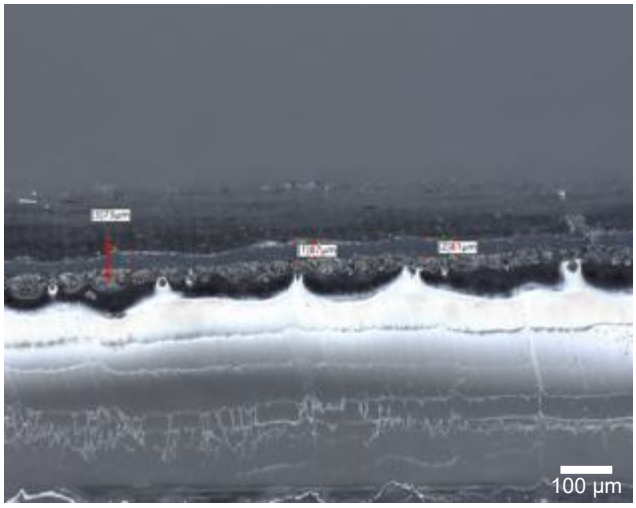

Figure **3-5**: Thickness of spin-coated PDMS on top of transferred LIG.

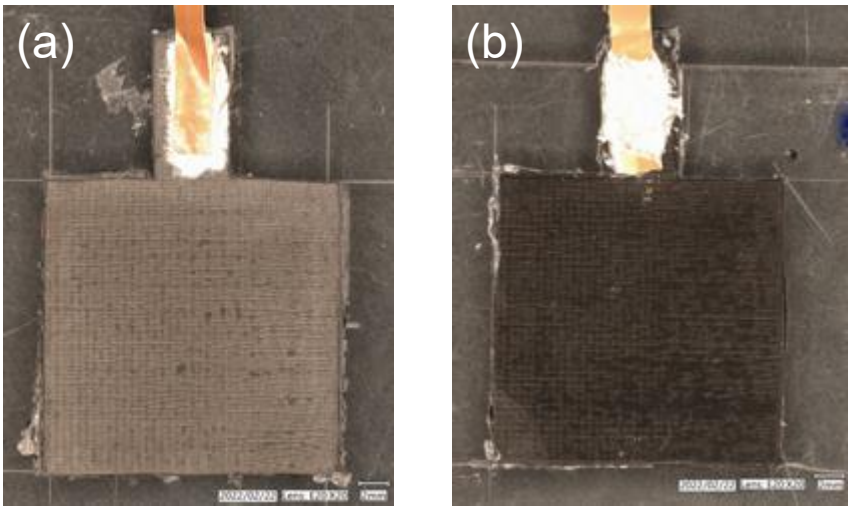

Figure **3-6**: (a)Completed smooth 2cm x 2cm LIG electrode. (b) Completed smooth 2cm x 2cm LIG electrode with PDMS.

3.2 Testing of the Smooth LIG TENG

The TENG was then connected to a Keithley 2100 multimeter and set up on a linear stage to test. The linear stage was calibrated so that the most consistent current

generation occurred when the two electrodes came together. The TENG was cycled at 0.75Hz - 1Hz because that was the highest frequency the linear stage could cycle. The linear stage setup and Arduino controller setup can be seen in Figure **A-7** and Figure **A-8** in Appendix A. A bridge rectifier was created using four diodes connected in a square pattern on a breadboard to filter out the negative current. The red wires are connected to the TENG output, and the yellow wires are connected to the multimeter, as seen in Figure **3-7**. The output from one of the test runs using the bridge rectifier can be seen in Figure **3-8.** The TENG had a maximum current generation of 280nA through the five best cycles. Also, the output of the TENG was almost cut in half after only 200 cycles. The output is shown in Figure **3-9a,** where the output was about 100nA after 50 cycles. Then in Figure **3-9b,** the output was reduced to less than half after 200 cycles. The reason for this will be examined further in the discussion chapter.

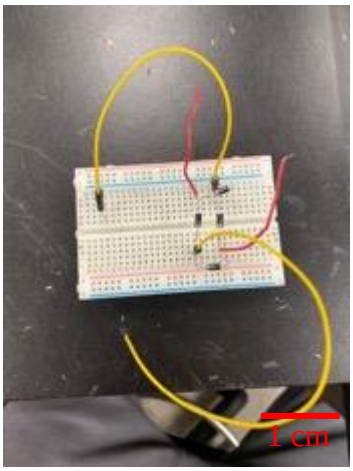

Figure **3-7**: Image of bridge rectifier made in a breadboard.

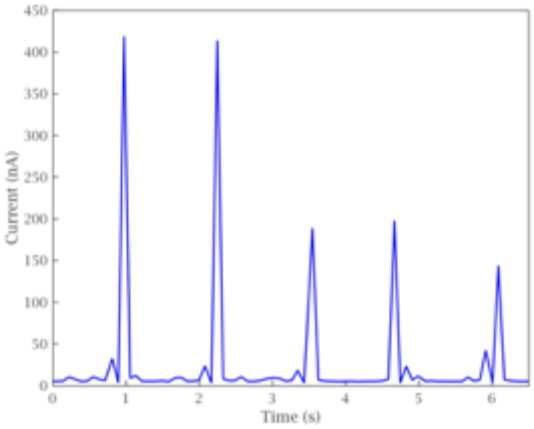

Figure **3-8**: Rectified current output of smooth LIG PDMS TENG at 0.75Hz.

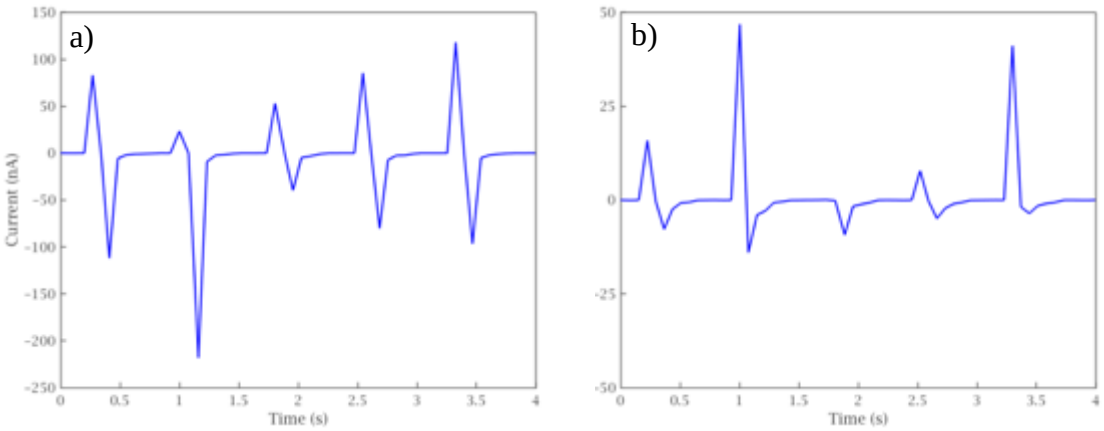

Figure **3-9**: The current output of smooth LIG PDMS TENG at 1Hz after 50 cycles. The current output of smooth LIG PDMS TENG at 1Hz after 200 cycles.

Chapter 4

Smooth LIG/AgNW Triboelectric Nanogenerator

4.1 Fabrication of Smooth LIG/AgNW based TENG

The smooth LIG/AgNW TENG electrodes were fabricated the same way as the smooth LIG electrodes described in Chapter **3.1** until the contacts were created. They were 2cm x 2cm electrodes with an extra 1cm x .5cm area to attach the contact. The steps in Figure **4-1a,b,c** are the same as in Figure **3-3a,b,c**. Before the contacts were added to the electrode using the procedure mentioned in Chapter 3, 60nm diameter AgNWs were spray-coated on the surface of the LIG. The spray-coating was done by diluting the commercial AgNW with IPA to a 1:3 dilution. Next, the AgNWs were vibrated for 2mins to mix the AgNWs and IPA thoroughly. Next, the AgNWs were spray coated onto the LIG by hand. Two coats of four passes were made on the LIG surface with a pressure of 30psi. Next, the AgNWs were cured at 60°C for 10mins to evaporate the IPA after each coat, as shown in Figure **4-1d**. The same contacts were put on the LIG/AgNW electrode using a two-part commercial Ag paste and strips of copper foil. The same procedure was followed as described in Chapter 3. The PDMS was then spin-coated on top of the LIG/AgNW electrode Figure **4-1e**. PVA, a triboelectric positive material, was spin-coated on top of the positive electrode at 2000RPM and 30 seconds Figure **4-1f**. These parameters yielded a 1-2μm thick layer of PVA on top of the AgNWs measured by an optical microscope. The PVA was added to protect the AgNWs and prevent them from

rubbing off the LIG. Spray coating the AgNWs greatly improved the sheet resistance of the LIG electrode, as seen in Table **4-1**. After doing the spray coating, the sheet resistance went from about 18Ω down to less than 6 Ω after doing the spray coating.

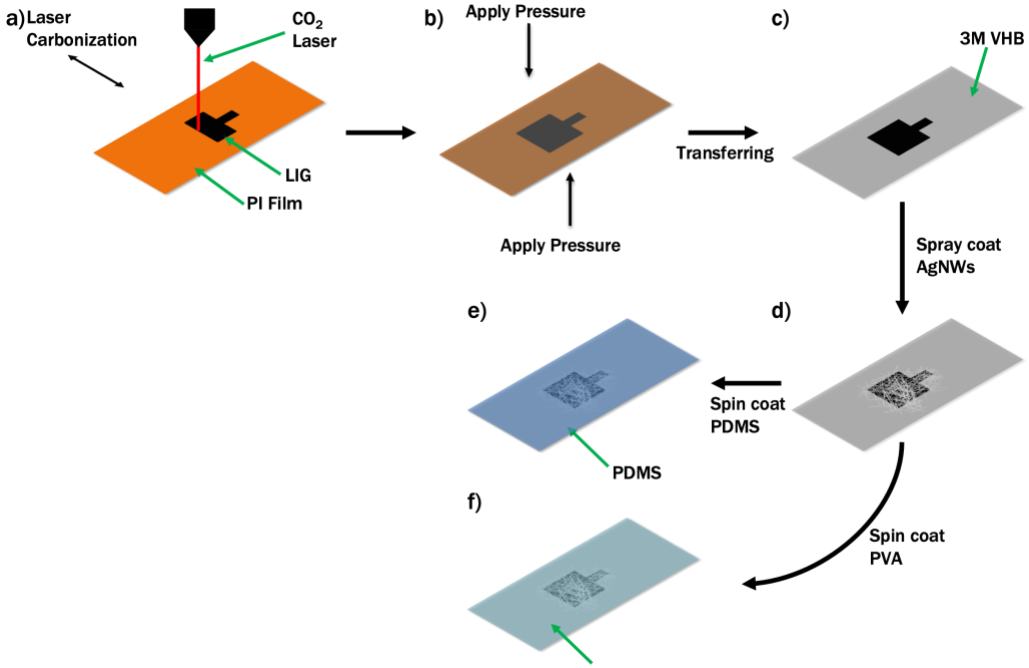

Figure **4-1**: Fabrication of the smooth LIG/AgNW TENG.

Table **4-1**: Resistance of LIG electrodes on 3m VHB tape from the top to the bottom of the electrodes before and after spray coating AgNWs on top.

Sample #	Resistance before AgNW (Ω)	Resistance After AgNW (Ω)
3	**17.8**	**3**
4	**19.1**	**5**

SEM images were also taken to see the microstructure of the AgNWs. In Figure **4-2a,b,c,** the AgNWs are seen connecting the microcracks in the LIG. They form a robust network of AgNWs that attach to the LIG, improving the LIG electrode. The length of each AgNW is 10s of microns long, allowing for them to span over 20µm gaps of the

microcracks. The finished positive electrode with PVA can be seen below in Figure **4-3a** and the negative electrode with PDMS in Figure **4-3b**.

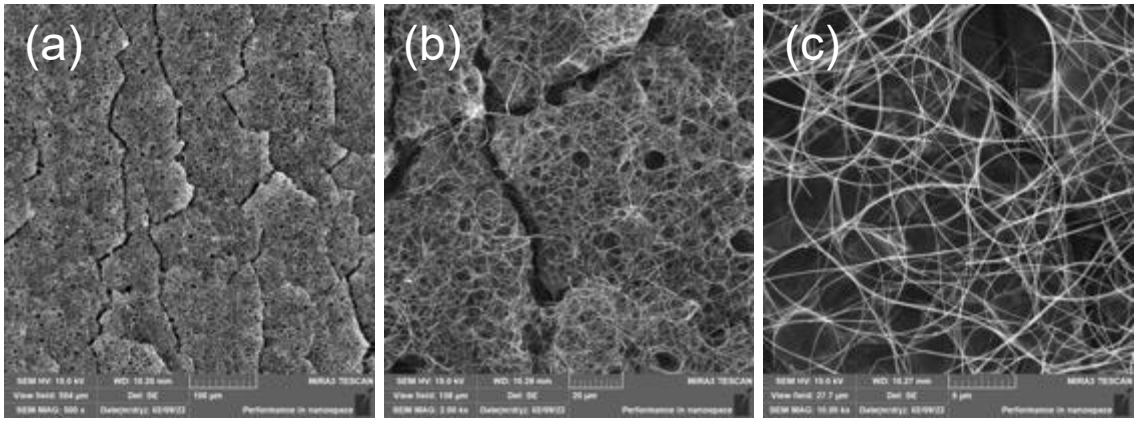

Figure **4-2**: (a) SEM image of AgNWs spray-coated on smooth LIG 500x. (b) SEM image of AgNWs spray-coated on smooth LIG 2,000x. (c) SEM image of AgNWs spray-coated on smooth LIG 10,000x

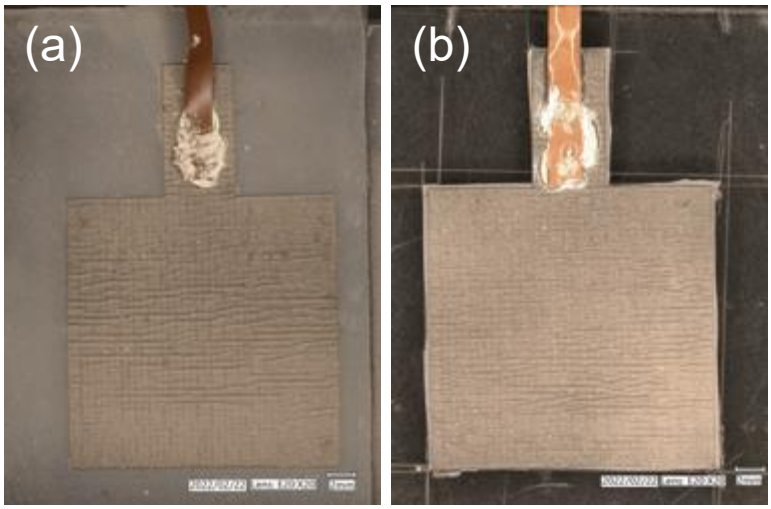

Figure **4-3**: (a) Stitched optical image of smooth LIG/AgNW electrode with PVA. (b) Stitched optical image of smooth LIG/AgNW electrode with PDMS.

4.2 Performance of the Smooth LIG/AgNW TENG

The TENG was tested using the same setup described in Chapter **3.2,** using the bridge rectifier and 0.75Hz cycle frequency. The best five cycles can be seen by testing the smooth LIG/AgNW TENG below in Figure **4-4**. The smooth LIG/AgNW had a maximum current output of 333nA.

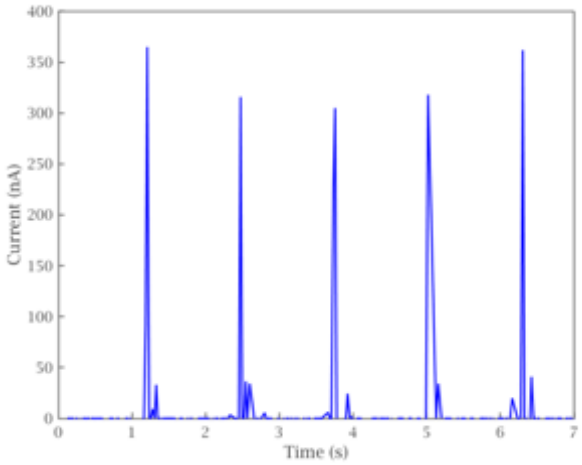

Figure **4-4**: Rectified current output of smooth LIG/AgNW PDMS TENG at 0.75Hz.

Chapter 5

Crumpled LIG/AgNW Based Triboelectric Nanogenerator

5.1 Fabrication of Crumpled LIG/AgNW TENG

The crumpled LIG/AgNW TENG fabrication starts with the CO_2 laser converting the PI film into LIG. The electrode area was 4cm in length and 1.5cm in width to obtain final dimensions of 2cm x 2cm once the LIG is transferred to the strained 3M VHB tape. The laser power and speed were kept at 19% and 11%, respectively, Figure **5-1a**. Once the LIG was fabricated on the PI, a piece of 3M VHB was cut to size to cover the printed LIG adequately. Then the VHB tape was taken by hand, stretched to 100% of its initial length, and placed on the LIG. A clamp was then used to apply pressure on the VHB tape for 2 minutes across the entire area of the LIG Figure **5-1b**. Next, the clamp was removed, and the VHB tape was grabbed on one side and ripped off in one continuous motion. As the LIG transferred to the LIG, the 100% strain was released in the VHB tape, forming a crumpled structure in Figure **5-1c**. Next, the VHB tape with the LIG was attached to a manual linear stage and stretched back to 100% of its original length to prepare for spray coating. After the transfer, AgNWs were spray-coated on the surface of the LIG to improve the conductivity. The AgNWs were prepared the same way described in Chapter **4.1**. The spray coating was done using a handheld spray coater at 30psi. In order to maximize the effectiveness of the AgNWs, two coats were applied, each consisting of four passes. The first coat was applied while the VHB was attached to the

linear stage and strained 100%. The AgNWs were then cured at 60°C for 10mins to evaporate the IPA. Then the strain was released, and another four passes of AgNWs were spray-coated on the LIG and cured at 60°C for 10mins shown in Figure **5-1d**. After the spray coating of AgNWs, the same contacts consisting of Ag paste and copper foil were created on the electrodes. Next, the positive and negative electrodes were created. The fabrication started by first spin-coating PDMS at 2000rpm and 30s on the crumpled LIG/AgNW surface. This higher rpm was chosen to maintain the crumpled structure of the LIG underneath. Similarly, the PVA was spin-coated on another crumpled LIG/AgNW electrode to protect the AgNWs. The two completed positive electrodes with PVA can be seen below in Figure **5-2a**. The completed negative electrode with PDMS can be seen below in Figure **5-2b**.

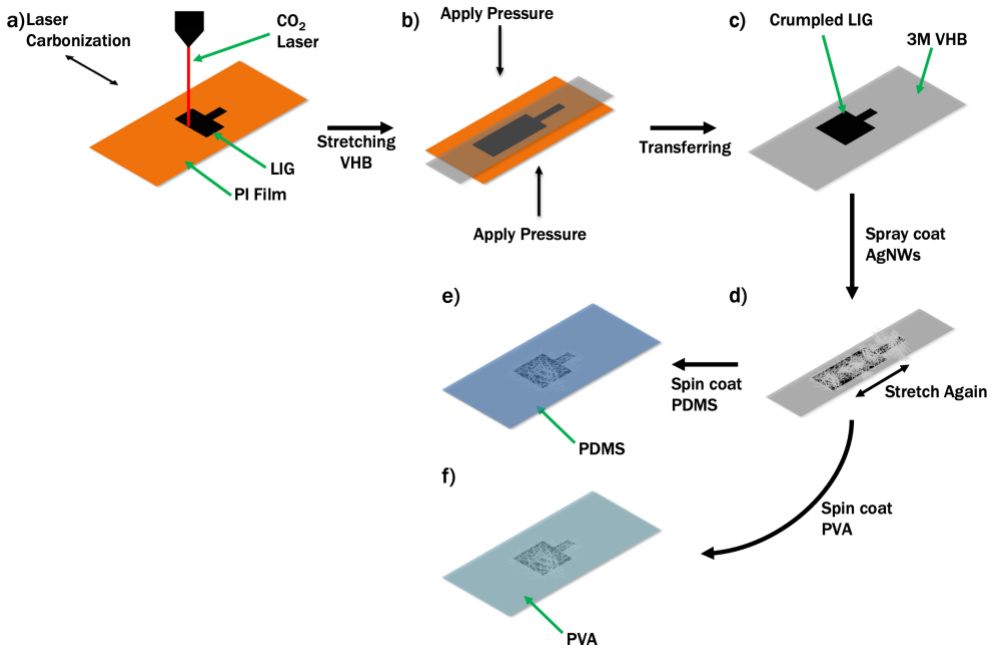

Figure **5-1**: Fabrication of the crumpled LIG/AgNW TENG.

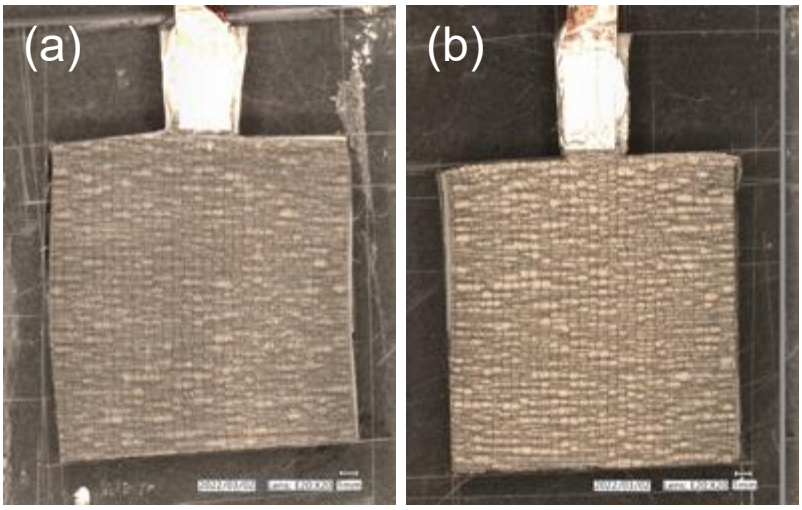

Figure **5-2**: (a) Stitched optical image of crumpled LIG/AgNW electrode with PVA 20x. (b) Stitched optical image of crumpled LIG/AgNW electrode with PDMS 20x.

SEM images of the crumpled LIG surface were taken to examine the microstructure. The LIG was crumpled perpendicular to the direction of the raster pattern to ensure consistent buckling in the LIG. The LIG buckled along the raster lines of the laser Figure **5-3a**. After the buckling, the LIG cracked into fragments that were no longer connected, leaving gaps between the fragments where the VHB tape was visible. Since the strain was released quickly from the transfer process, the fragments stacked on top of each other Figure **5-3b**. The LIG did still retain its porous structure through the transferring. The thickness of the crumpled structure was measured through a cross-sectional optical image. The amplitude of the buckles was 155μm, with their wavelength being 100μm, as seen in Figure **5-4**. The spray-coating of AgNWs was also studied by SEM to ensure they evenly covered the surface of the crumpled LIG to increase the conductivity of the electrode. Figure **5-5a** shows the AgNWs across the entire crumpled surface, with the crumpled structure still clearly being visible. Figure **5-5b** shows a more magnified image of a peak of one of the buckles with the AgNWs coated on top.

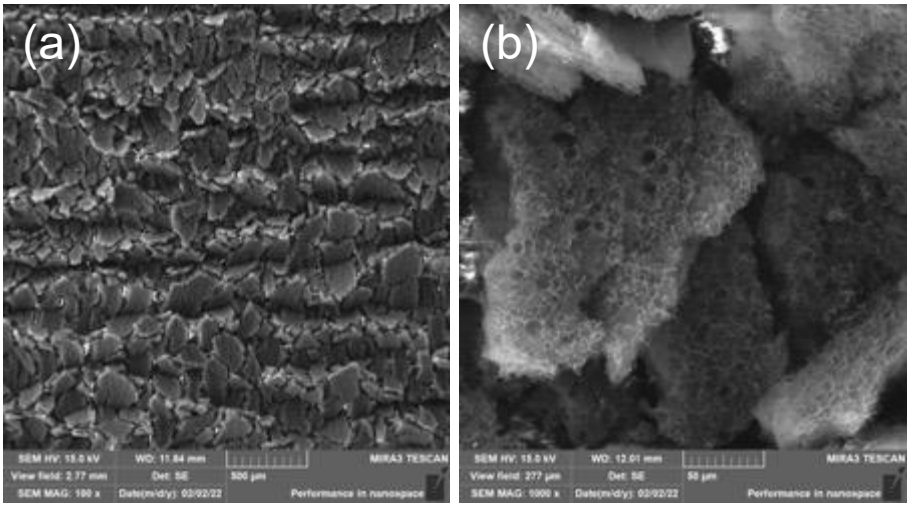

Figure **5-3**: (a) SEM image of the crumpled LIG with 100%pre-strain 100x. (b) SEM image of the crumpled LIG with 100% pre-strain 1000x

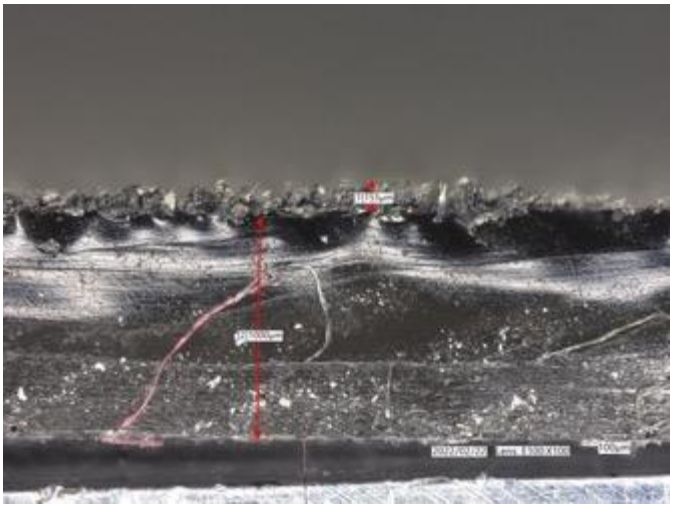

Figure **5-4**: Optical image of the thickness of crumpled LIG on VHB 100x.

The continuity of the AgNWs is seen between the LIG fragments by looking at a more magnified view of the surface in Figure **5-5c**. The porous structure is visible in the LIG, while the AgNWs connect the two fragments together. The thickness of the AgNW layer can also be seen, which is about 1-2μm. While the coverage of the AgNWs is not consistent since they were spray-coated by hand.

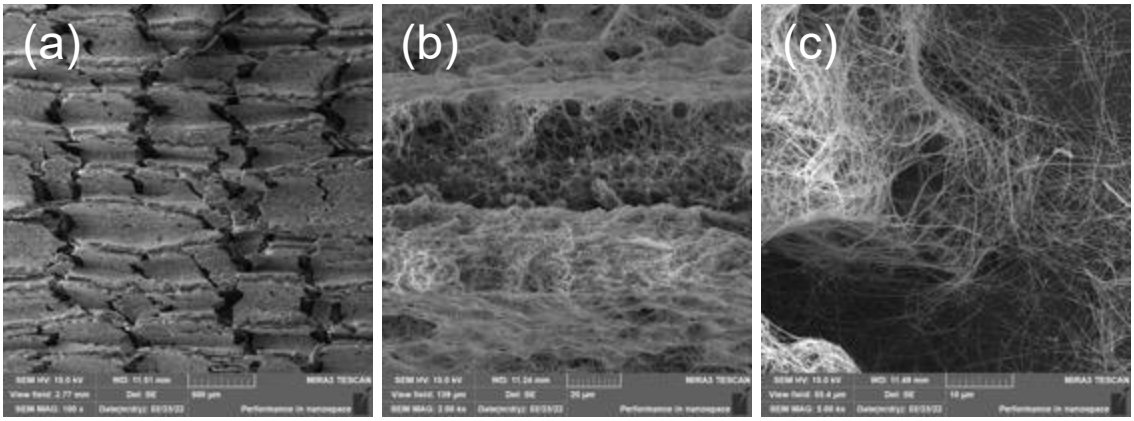

Figure **5-5**: (a) SEM image of the crumpled LIG with AgNW spray-coating 100x. (b) SEM image of the crumpled LIG with AgNW 2,000x. (c) SEM image of the crumpled LIG with AgNW 5,000x.

5.2 Performance of Crumpled LIG/AgNW TENG

The performance of the crumpled LIG/AgNW TENG was evaluated through cyclic resistance measurements to analyze the robustness of the device for on-body applications. The current output of the device was also filtered by a bridge rectifier and measured by a multimeter. In order to measure the resistance of the electrode, the crumpled LIG/AgNW was attached to a manual linear stage. Next, the electrode was stretched to 100% of its original length up to ten times. The resistance was then measured with a voltmeter from the top and bottom of the electrode during the stretched and unstretched state. The distance between the voltmeter probes was kept at 2cm since resistance scales linearly. The results from that cyclic testing are seen below in Figure **5-6**, and the resistance from those measurements was stable between 16Ω and 20Ω. While these resistance measurements are robust like a TLM or four-probe method, they provide

data that the conductivity of the electrodes is primarily independent of strain on the system.

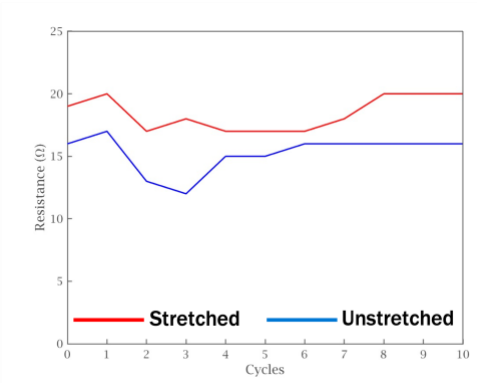

Figure **5-6**: Resistance measurements of the crumpled LIG/AgNW TENG after ten cycles to a strain of 100%.

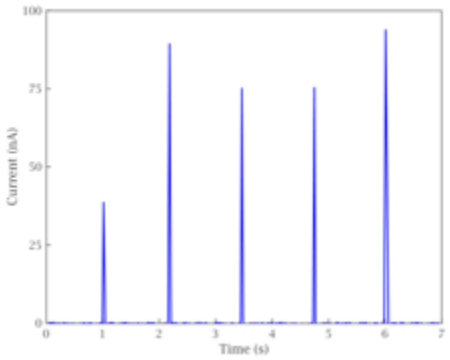

Figure **5-7**: Rectified current output of the crumpled LIG/AgNW PDMS TENG at 0.75Hz.

Chapter 6

Discussion

6.1 Smooth LIG TENG

The quality of the printed LIG was sufficient for consistent and highly conductive LIG after transferring to the 3M VHB for the smooth LIG TENG and the smooth LIG/AgNW TENG. While the LIG did show microcracks after transferring, it only increased the resistance by 7-12Ω after transferring (Table **3-1**). The LIG also maintained its porosity after transferring despite the pressure applied by the clamp. This porosity allowed it to receive the spray coating of the AgNWs better. Also, the thickness of the LIG did almost double during transferring according to the SEM cross-sections. The doubling of the thickness was probably caused during the transferring process. The LIG slightly separates when it is pulled from the PI tape. The smooth LIG TENG did have significantly lower output values than those previously reported in the literature.[3] It is also lower than comparable CVD graphene-based TENGs that use the same PDMS negative triboelectric material.[37] The lower output is thought to be because of the transferring process itself, reducing the quality of the LIG electrode and not getting a perfectly uniform contact between the LIG and PDMS, and the decay of current output observed. After just 200 cycles, the output from the smooth LIG TENG decreased by over 50%. This reduction was caused by the LIG adhering to the PDMS as it made contact, thus reducing the effective surface area of the TENG. After those 200 cycles, the

LIG was visible on the surface of the PDMS and could not be thoroughly cleaned off the surface of the PDMS using solvents. The LIG adhering to the PDMS ultimately led to less charge being transferred between the two sides of the device.

6.2 Smooth LIG/AgNW TENG

The spray coating of the AgNWs significantly increased the conductivity of LIG electrode. The AgNWs adhered to the LIG well enough to reduce the resistance, which ultimately was reflected in the device's output, which was higher than the smooth LIG TENG without AgNWs. The AgNWs did not have the best adhesion to the LIG, and their connection was very fragile. The AgNWs could be wiped off easily if anything was rubbed across the surface. This is why the very thin layer of PVA was needed to keep the AgNWs in place and prevent them from leaving the LIG and compromising the integrity of the electrode. PVA was chosen because it is a triboelectric material that would not drastically affect the TENG's performance. With that being said, the performance of the LIG/AgNW was tested without the PVA, so I cannot make that statement definitively. The PDMS on the negative electrode protected the AgNWs the same way the PVA did on the positive electrode. It is also worth mentioning that the 60nm AgNWs were chosen arbitrarily because that was the diameter of AgNW that was available in the lab at the time. Using different larger diameter AgNW could lower the resistance and increase the output further. The output of this device was also still lower than other LIG TENGs in the literature.[3]

6.3 Crumpled LIG/AgNW TENG

The buckling of the LIG using a prestrain strategy was successful as the first attempt ever done in literature but had much room for improvement. This is especially true since the original goal was to create a crumpled LIG TENG without AgNWs, but the AgNWs were needed to help feel the gaps in the LIG. The main problem of the buckling of the LIG came because the LIG was brittle, and the strain was released very quickly. Since LIG is thicker and the quality of the graphene is lower than chemical vapor deposition graphene, the LIG is less flexible and cannot withstand the quick releasing of the strain. Releasing the strain quickly also caused the LIG to detach from the VHB tape. Since the LIG cracked and released from the VHB, the fragments of LIG stacked on top of each other, significantly reducing the conductivity of the entire electrode. The AgNWs were then added to increase this conductivity and improve the stretchability of the TENG electrode, which they did. This crumpled structure did not increase the output of the TENG as I initially hypothesized. It instead had an output over 200nA lower than the other two devices, as can be seen in the comparison in Figure **6-1**. This decrease is thought to be caused by the poor quality of the crumpled LIG structure and the amplitude of the crumpled structure being too large. The first reason is thought to be true because even though the AgNWs significantly improved the conductivity of the electrode, they did not improve the conductivity of the electrode directly. They only added a conducting layer on top of the LIG, effectively making the electrode an AgNW electrode instead of a crumpled LIG electrode with some AgNWs on top. On the other hand, the large crumples caused the contact area between the two materials to decrease rather than increase

because the scale of the structures was too large. Since the amplitude of the crumples was over 155µm, the PDMS negative electrode could not effectively conform to features that large and make consistent contact across the electrode. This loss in contact drastically reduced the contact area, thus decreasing the charges transferred.

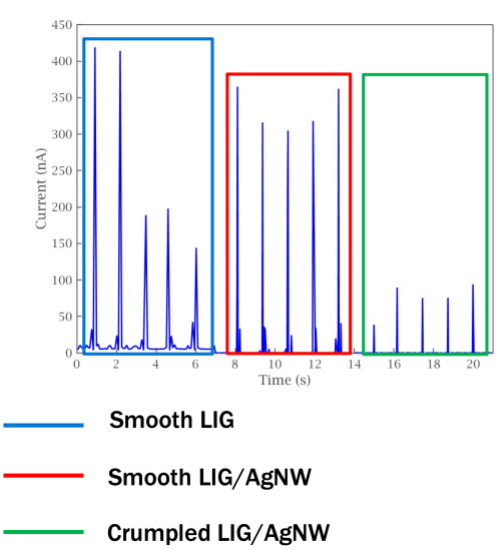

Figure **6-1**: Rectified current output at 0.75Hz for the smooth LIG TENG in blue, smooth LIG/AgNW TENG in red, and crumpled LIG/AgNW TENG in green.

Chapter 7

Conclusion and Future Work

Using LIG, AgNWs, and a prestrain strategy, a working crumpled LIG/AgNW TENG was successfully fabricated and produced the triboelectric effect for harvesting mechanical energy. Three different TENGs were created to compare the difference in performance and the effect the addition of AgNWs and a crumpled structure had on the output of the TENG. Each device's microstructure was examined using an SEM and optical microscope. The current outputs of the devices were tested using a linear stage, bridge rectifier, and multimeter. The smooth LIG TENG was used as the control device, and the smooth LIG/AgNW TENG and crumpled LIG/AgNW TENG were compared against it. The smooth LIG TENG control device had the second-highest output out of the three devices. The main problem with the device was that the LIG would adhere to the PDMS material on the other side. This adhesion of LIG caused a decrease in performance that manifested itself after only 200 cycles. In the future, a method of coating the LIG with a protective layer such as PVA could be investigated to solve this problem. Also, removing the loose top layer of LIG could be attempted by attaching an adhesive tape that would remove the loose layer. Also, further investigation of the contacts needs to be done since the output of this smooth LIG TENG with PDMS was lower than other LIG TENGs in the literature.[3]

The smooth LIG/AgNW TENG had the highest output of the three devices. This is thought to be due to the reduction in resistance after adding AgNWs to the surface.

This reduction in resistance would allow the charge to transfer more easily across the electrode. More investigation into this hypothesis needs to be done to confirm it, including better electrical characterization of the contacts and the interface between the LIG and AgNWs. Since the AgNWs did not adhere well to the surface of the LIG, PVA was added to protect them. The effect of PVA on the output of the TENG was never tested. This effect needs to be investigated further in the future by fabricating a device with and without PVA and testing their outputs.

Finally, while this was the first time in literature that a crumpled LIG structure was successfully fabricated as part of a TENG and tested, it had many areas that can be improved. The first problem that caused the others was the low output of the device that was caused by the chaotic buckling of the LIG. The mechanisms behind this buckling need to be researched further to improve the process. The first is finding a way to release the strain slowly, so the LIG does not become unattached from the VHB. The second would be to change the morphology of the fabricated LIG by changing the laser parameters to create a thinner and more robust LIG layer. The thinner and more robust LIG layer would allow it to be more resistant to cracking and make it more flexible. Also, more cyclic mechanical tests are needed for the TENG to show that it can withstand 100s or 1000s of stretching cycles without a degradation in performance. Finally, a more controlled testing setup with better contacts and even a faraday cage could be added to reduce the noise in the system and obtain a more accurate output of the TENG. While the results presented in this thesis are not perfect, they provide a steppingstone and lessons learned for the future improvement of this device.

References

[1] J. Liu, L. Zhang, N. Wang, and C. Li, “Highly stretchable and transparent triboelectric nanogenerator based on multilayer structured stable electrode for self-powered wearable sensor,” *Nano Energy*, vol. 78, no. September, p. 105385, 2020, doi: 10.1016/j.nanoen.2020.105385.

[2] H. Chen, Y. Xu, J. Zhang, W. Wu, and G. Song, “Enhanced stretchable graphene-based triboelectric nanogenerator via control of surface nanostructure,” *Nano Energy*, vol. 58, no. September 2018, pp. 304–311, 2019, doi: 10.1016/j.nanoen.2019.01.029.

[3] H. Chen, X. Ding, and B. Zheng, “stretchable sensing platform based on laser-induced graphene foams Human motion-driven self-powered stretchable sensing platform based on laser-induced graphene foams,” vol. 011413, no. November 2021, 2022, doi: 10.1063/5.0077667.

[4] A. Lamberti, F. Clerici, M. Fontana, and L. Scaltrito, “A highly stretchable supercapacitor using laser-induced graphene electrodes onto elastomeric substrate,” *Advanced Energy Materials*, vol. 6, no. 10, pp. 1–6, 2016, doi: 10.1002/aenm.201600050.

[5] C. Zhang *et al.*, “High-energy all-in-one stretchable micro-supercapacitor arrays based on 3D laser-induced graphene foams decorated with mesoporous ZnP nanosheets for self-powered stretchable systems,” *Nano Energy*, vol. 81, no. November 2020, p. 105609, 2021, doi: 10.1016/j.nanoen.2020.105609.

[6] M. G. Stanford, J. T. Li, Y. Chyan, Z. Wang, W. Wang, and J. M. Tour, “Laser-Induced Graphene Triboelectric Nanogenerators,” *ACS Nano*, vol. 13, no. 6, pp. 7166–7174, 2019, doi: 10.1021/acsnano.9b02596.

[7] P. He, Y. Peng, and L. Lin, “A Multimodal Self-Healing Flexible Sweat Sensor for Healthcare Monitoring,” *Proceedings of the IEEE International Conference on Micro Electro Mechanical Systems (MEMS)*, vol. 2021-Janua, no. January, pp. 517–520, 2021, doi: 10.1109/MEMS51782.2021.9375234.

[8] J. Lin *et al.*, “Laser-induced porous graphene films from commercial polymers,” *Nature Communications*, vol. 5, pp. 5–12, 2014, doi: 10.1038/ncomms6714.

[9] J. Zhu *et al.*, “Stretchable wideband dipole antennas and rectennas for RF energy harvesting,” *Materials Today Physics*, vol. 18, p. 100377, 2021, doi: 10.1016/j.mtphys.2021.100377.

[10] M. Parmeggiani *et al.*, “PDMS/Polyimide Composite as an Elastomeric Substrate for Multifunctional Laser-Induced Graphene Electrodes,” *ACS Applied Materials and Interfaces*, vol. 11, no. 36, pp. 33221–33230, 2019, doi: 10.1021/acsami.9b10408.

[11] Q. Li, T. Wu, W. Zhao, J. Ji, and G. Wang, “Laser-Induced Corrugated Graphene Films for Integrated Multimodal Sensors,” *ACS Applied Materials and Interfaces*, 2021, doi: 10.1021/acsami.1c12686.

[12] H. Jiang, D. Y. Khang, J. Song, Y. Sun, Y. Huang, and J. A. Rogers, “Finite deformation mechanics in buckled thin films on compliant supports,” *Proceedings of the National Academy of Sciences of the United States of America*, vol. 104, no. 40, pp. 15607–15612, 2007, doi: 10.1073/pnas.0702927104.

[13] S. Chattopadhyay, “Biaxially Stretchable ‘Wavy’ Silicon Nanomembranes on Elastomeric Supports Fabricated,” *MRS Bulletin*, vol. 32, no. 8, p. 606, 2007, doi: 10.1557/mrs2007.117.

[14] J. Song, H. Jiang, W. M. Choi, D. Y. Khang, Y. Huang, and J. A. Rogers, “An analytical study of two-dimensional buckling of thin films on compliant substrates,” *Journal of Applied Physics*, vol. 103, no. 1, 2008, doi: 10.1063/1.2828050.

[15] Y. Sun, W. M. Choi, H. Jiang, Y. Y. Huang, and J. A. Rogers, “Controlled buckling of semiconductor nanoribbons for stretchable electronics,” *Nature Nanotechnology*, vol. 1, no. 3, pp. 201–207, 2006, doi: 10.1038/nnano.2006.131.

[16] C. Yu, K. O’Brien, Y. H. Zhang, H. Yu, and H. Jiang, “Tunable optical gratings based on buckled nanoscale thin films on transparent elastomeric substrates,” *Applied Physics Letters*, vol. 96, no. 4, 2010, doi: 10.1063/1.3298744.

[17] Y. Wang *et al.*, “Super-elastic graphene ripples for flexible strain sensors,” *ACS Nano*, vol. 5, no. 5, pp. 3645–3650, 2011, doi: 10.1021/nn103523t.

[18] W. G. Kim, D. W. Kim, I. W. Tcho, J. K. Kim, M. S. Kim, and Y. K. Choi, “Triboelectric Nanogenerator: Structure, Mechanism, and Applications,” *ACS Nano*, vol. 15, no. 1. American Chemical Society, pp. 258–287, Jan. 26, 2021. doi: 10.1021/acsnano.0c09803.

[19] “Is Water Necessary for Contact Electrification? - Baytekin - 2011 - Angewandte Chemie - Wiley Online”.

[20] A. F. Diaz and R. M. Felix-Navarro, “A semi-quantitative tribo-electric series for polymeric materials: The influence of chemical structure and properties,” *Journal*

of Electrostatics, vol. 62, no. 4, pp. 277–290, 2004, doi: 10.1016/j.elstat.2004.05.005.

[21] S. H. Shin *et al.*, "Formation of Triboelectric Series via Atomic-Level Surface Functionalization for Triboelectric Energy Harvesting," *ACS Nano*, vol. 11, no. 6, pp. 6131–6138, 2017, doi: 10.1021/acsnano.7b02156.

[22] J. Chen *et al.*, "Metal-Ion Coupling in Metal–Organic Framework Materials Regulating the Output Performance of a Triboelectric Nanogenerator," *Inorganic Chemistry*, 2022, doi: 10.1021/acs.inorgchem.1c03338.

[23] S. Niu *et al.*, "Theoretical study of contact-mode triboelectric nanogenerators as an effective power source," *Energy and Environmental Science*, vol. 6, no. 12, pp. 3576–3583, 2013, doi: 10.1039/c3ee42571a.

[24] V. Nguyen and R. Yang, "Effect of humidity and pressure on the triboelectric nanogenerator," *Nano Energy*, vol. 2, no. 5, pp. 604–608, 2013, doi: 10.1016/j.nanoen.2013.07.012.

[25] G. Xu *et al.*, "Density of Surface States: Another Key Contributing Factor in Triboelectric Charge Generation," *ACS Applied Materials & Interfaces*, vol. 14, no. 4, pp. 5355–5362, 2022, doi: 10.1021/acsami.1c21359.

[26] W. Zhang *et al.*, "Measuring the actual voltage of a triboelectric nanogenerator using the non-grounded method," *Nano Energy*, vol. 77, no. June, p. 105108, 2020, doi: 10.1016/j.nanoen.2020.105108.

[27] F. R. Fan, Z. Q. Tian, and Z. Lin Wang, "Flexible triboelectric generator," *Nano Energy*, vol. 1, no. 2, pp. 328–334, Mar. 2012, doi: 10.1016/j.nanoen.2012.01.004.

[28] S. H. Ji, W. Lee, and J. S. Yun, “All-in-One Piezo-Triboelectric Energy Harvester Module Based on Piezoceramic Nanofibers for Wearable Devices,” *ACS Applied Materials and Interfaces*, vol. 12, no. 16, pp. 18609–18616, 2020, doi: 10.1021/acsami.0c02754.

[29] C. Jirayupat *et al.*, “Piezoelectric-Induced Triboelectric Hybrid Nanogenerators Based on the ZnO Nanowire Layer Decorated on the Au/polydimethylsiloxane-Al Structure for Enhanced Triboelectric Performance,” *ACS Applied Materials and Interfaces*, vol. 10, no. 7, pp. 6433–6440, 2018, doi: 10.1021/acsami.7b17314.

[30] Z. Ren *et al.*, “Trapezoidal Cantilever-Structure Triboelectric Nanogenerator Integrated with a Power Management Module for Low-Frequency Vibration Energy Harvesting,” *ACS Applied Materials & Interfaces*, vol. 14, no. 4, pp. 5497–5505, 2022, doi: 10.1021/acsami.1c23309.

[31] X. S. Zhang *et al.*, “Frequency-multiplication high-output triboelectric nanogenerator for sustainably powering biomedical microsystems,” *Nano Letters*, vol. 13, no. 3, pp. 1168–1172, 2013, doi: 10.1021/nl3045684.

[32] W. Fan *et al.*, “A P P L I E D S C I E N C E S A N D E N G I N E E R I N G Machine-knitted washable sensor array textile for precise epidermal physiological signal monitoring,” 2020. [Online]. Available: https://www.science.org

[33] M. Xu *et al.*, “High Power Density Tower-like Triboelectric Nanogenerator for Harvesting Arbitrary Directional Water Wave Energy,” *ACS Nano*, vol. 13, no. 2, pp. 1932–1939, Feb. 2019, doi: 10.1021/acsnano.8b08274.

[34] G. Zhu *et al.*, "Harvesting water wave energy by asymmetric screening of electrostatic charges on a nanostructured hydrophobic thin-film surface," *ACS Nano*, vol. 8, no. 6, pp. 6031–6037, Jun. 2014, doi: 10.1021/nn5012732.

[35] J. Li, Z. Zhang, X. Luo, L. Zhu, and Z. L. Wang, "Triboelectric Leakage-Field-Induced Electroluminescence Based on ZnS:Cu," *ACS Applied Materials & Interfaces*, vol. 14, no. 3, pp. 4775–4782, 2022, doi: 10.1021/acsami.1c23155.

[36] J. Luo, W. Gao, and Z. L. Wang, "The Triboelectric Nanogenerator as an Innovative Technology toward Intelligent Sports," *Advanced Materials*. John Wiley and Sons Inc, 2021. doi: 10.1002/adma.202004178.

[37] H. Chen, Y. Xu, J. Zhang, W. Wu, and G. Song, "Enhanced stretchable graphene-based triboelectric nanogenerator via control of surface nanostructure," *Nano Energy*, vol. 58. pp. 304–311, 2019. doi: 10.1016/j.nanoen.2019.01.029.

[38] J. T. Li, M. G. Stanford, W. Chen, S. E. Presutti, and J. M. Tour, "Laminated Laser-Induced Graphene Composites," *ACS Nano*, vol. 14, no. 7, pp. 7911–7919, 2020, doi: 10.1021/acsnano.0c02835.

[39] H. Wang, Z. Xiang, J. Wan, Y. Song, and H. Zhang, "Double-Sided Laser-Induced Graphene Based Smart Bracelet for Sensing and Energy," *Proceedings of the IEEE International Conference on Micro Electro Mechanical Systems (MEMS)*, vol. 2021-Janua, no. January, pp. 34–37, 2021, doi: 10.1109/MEMS51782.2021.9375415.

Appendix A

Supplementary Data

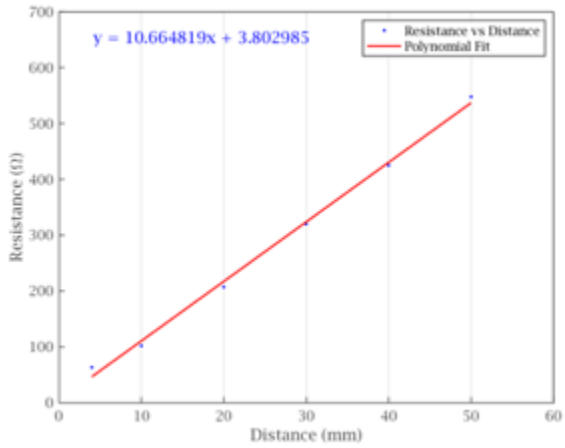

Figure **A-1**: TLM measurement of the long raster as printed LIG.

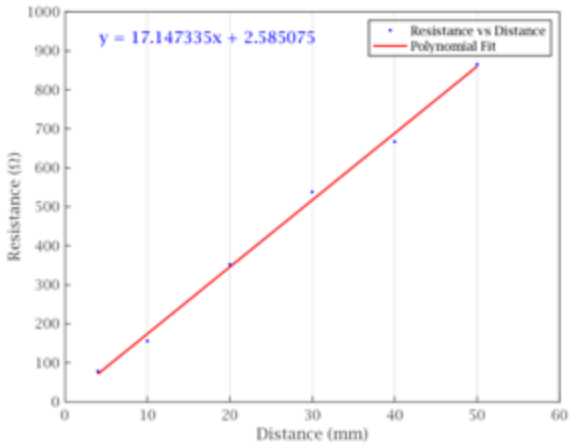

Figure **A-2**: TLM measurement of the short raster as printed LIG.

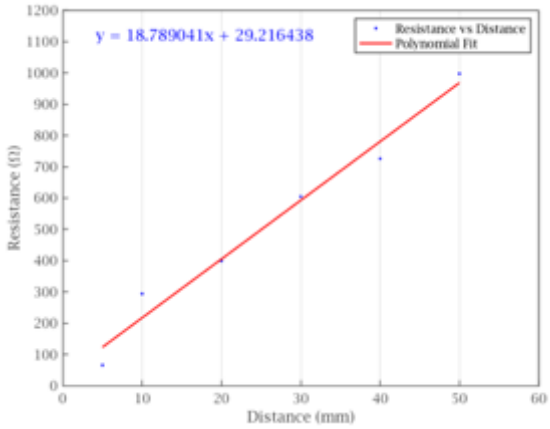

Figure **A-3**: TLM measurement of the long raster transferred LIG.

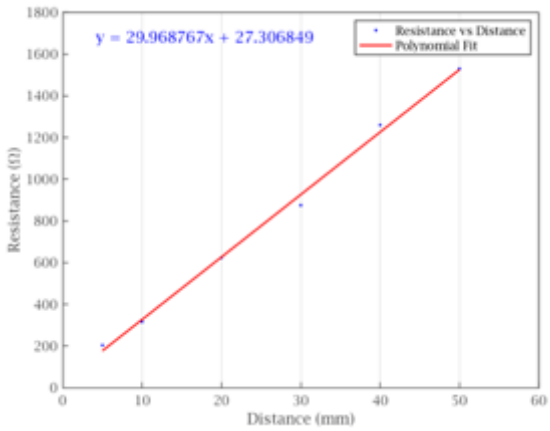

Figure **A-4**: TLM measurement of the short raster transferred LIG.

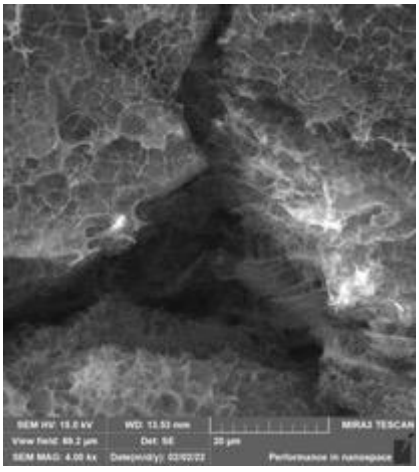

Figure **A-5**: Microstructure of transferred LIG on unstrained VHB tape 4000x.

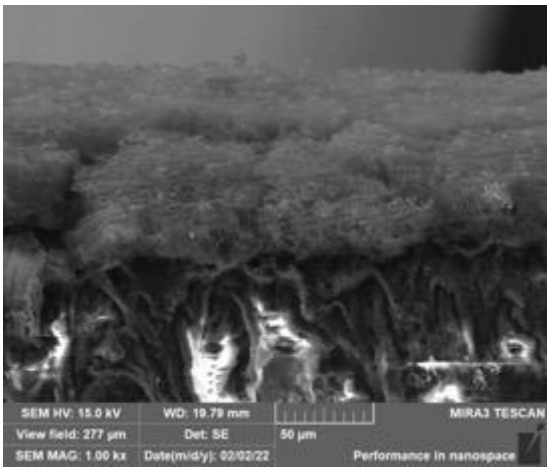

Figure **A-6**: Thickness measurement of the LIG transferred on the 3M VHB tape.

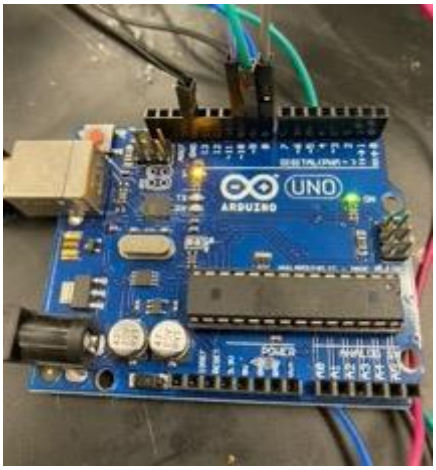

Figure **A-7**: Arduino board configuration for controlling the linear stage.

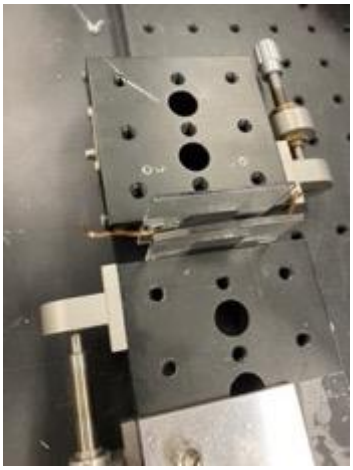

Figure **A-8**: TENG testing setup with the linear stage.

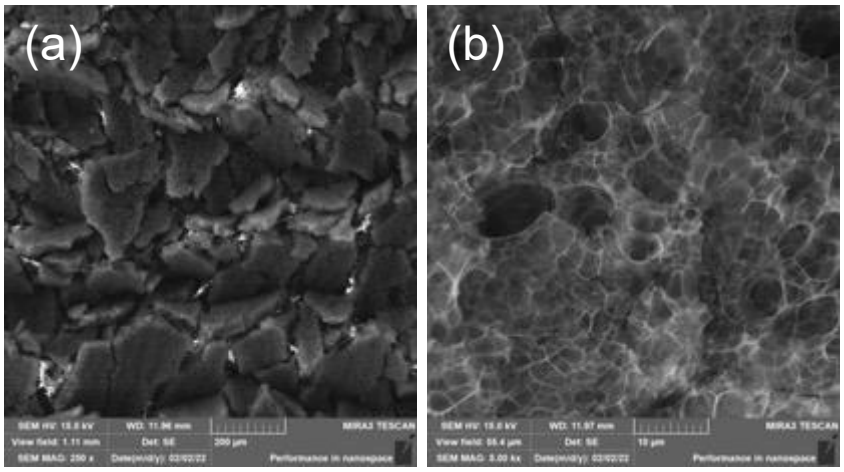

Figure **A-9**: (a) Crumpled LIG with 100% prestrained VHB 250x.

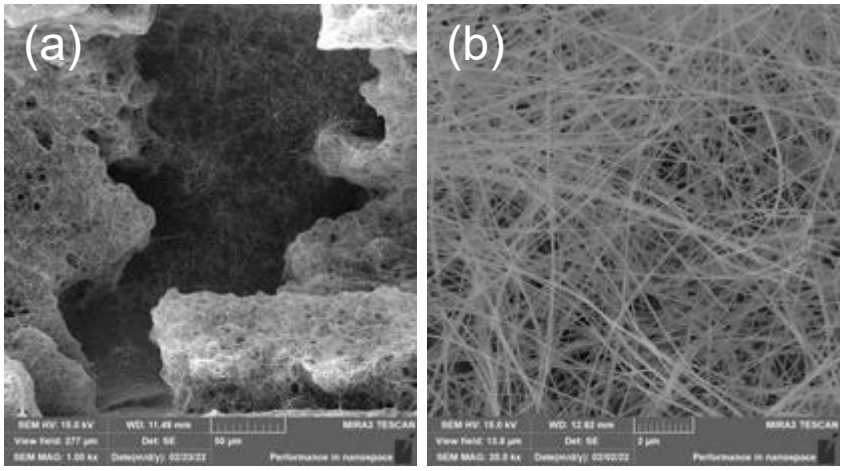

Figure **A-10**: Microstructure of spray-coated AgNWs on LIG on 100% strained VHB 4000x.

Appendix B

Non-Technical Abstract

The on-body wearable sensor field is a rapidly growing area of research that is already producing commercial products that can measure many of the wearer's physiological levels. While these devices have a lot of promise, one of the biggest problems to solve for their effectiveness is how they are powered. A prevalent phenomenon known as static electricity can be taken advantage of and used to produce an effect known as triboelectrification to solve this problem. The exchange of charges between two materials has been used to provide continuous power by converting mechanical energy into electrical energy. Here, three separate laser-induced graphene (LIG) and polydimethylsiloxane (PDMS) triboelectric nanogenerators (TENGs) were developed and tested to find an improved energy harvesting method. The first was constructed with simply LIG and PDMS. The second was built the same as the first but with silver nanowires (AgNWs) to aid in the charge transfer. Lastly, the third TENG was fabricated with AgNWs and LIG in a crumpled structure to increase the surface area of the surfaces in contact. The smooth LIG TENG had an output of 280nA but degraded quickly due to the LIG adhering to the PDMS. The smooth LIG/AgNW had the best output of 333nA due to the improved conductivity that the AgNWs provided. Finally, the crumpled LIG/AgNW TENG had the lowest output of 75nA because the size of the crumpled structure was too large, actually decreasing the contact surface area and thus

output. While these results are lower than reported literature values for similar LIG TENGs, it proves that a crumpled LIG TENG can be created and provide a foundation for crumpled LIG TENGs in the future.